Chem. Phys. Lipids 7 (1971) 207–230 © North-Holland Publishing Company

SYNTHESES AND NOVEL USES OF NITROXIDE MOTION PROBES

J. C. WILLIAMS, R. MEHLHORN and A. D. KEITH
Dept. of Genetics, University of California, Berkeley, Calif. 94720

Received April 24, 1971
Accepted June 1, 1971

A number of nitroxide spin lables of different molecular geometry were synthesized. These were used to infer the effect of molecular geometry and matrix ordering upon the extent of rotational anisotropy. Simulations were used in conjunction with selected spin labels to demonstrate that enhanced tumbling about the x- and y-principal axes of the nitroxide gives rise to unique spectra and can be recognized qualitatively.

I. Introduction

Spin label studies have been carried out on biological membranes relating to the matrix ordering of static systems[1–7]), local polarity as reflected by hyperfine coupling (A_N) or g-scalar shifts, and freedom of molecular motion[8–10]). Local matrix ordering of non-oriented samples has eluded investigators due to an inability to describe anisotropic motion. We describe anisotropic motion reflecting ordering in the matrix without imposing the necessity of mechanical ordering of the membrane system by hydrodynamic shear or fixed multilayers. Thus, the restrictions of sample orientation in the magnetic field and very slow molecular motion are removed. To accomplish our investigation of anisotropic motion, two areas of endeavor were explored. First, we synthesized a large variety of probes which vary as to polarity, conformation, chain length, and the geometry of spin-orbitals in relation to the molecular backbone. Secondly, the evolution of a mathematical description of molecular motion was undertaken with the aid of computer generated spectra in order to arrive at the physical basis of spectral types.

II. Experimental

The general use of mesylates in spin label chemistry is illustrated in fig. 1. Baumann and Mangold have generally developed the field of mesylate chemistry[11,12]) and the applications presented here illustrate the potential

for spin label chemistry. The Keana synthesis[13]) is shown in fig. 2 and represents a general method for synthesizing nitroxides on ketone sites.

Fig. 2 also shows a new general method for synthesizing oxazolidine rings at olefinic sites. Birkenbach and Linhard[14]) originally demonstrated the synthesis of β-iodiosocynates at double bond sites. Hassner et al.[15]) showed that the β-iodoisocynates could be ring-closed (by treatment with base) to form aziridines. Leonard et al.[16]) demonstrated the expansion of a number of aziridinium rings with acetone to yield oxazolidinium salts. The synthesis of 9,10NS demonstrates the expansion of an unsubstituted aziridine to an oxazolidine. Subsequent oxidation of this compound results in an N-oxyl

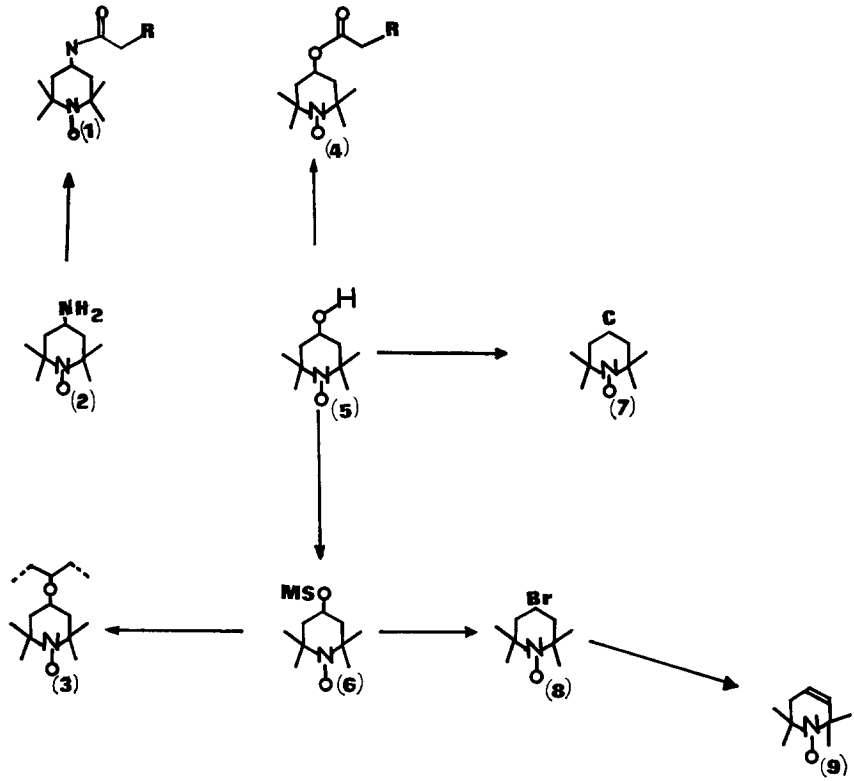

Fig. 1. Compound 5 (2,2,6,6-tetramethyl piperidinol-1N oxyl), TEMPOL. Compound 6 is the product after reaction with methane sulfonyl chloride. MS, the methyl sulfonic acid residue (methane sulfonyl TEMPOL, MST). Compound 3 shows the generalized product of ether formation from MST. Compound 8 shows the product after halogen formation by reaction with $MgBr_2$. Compound 9 shows the product of debromination of compound 8. Compound 7 shows the product of chlorination of TEMPOL. Compound 4 shows the product of ester formation by reaction of acid chlorides with TEMPOL. Compound 2 is the amine derivative of piperidine (2,2,6,6-tetramethyl piperidine-NH_2-1N oxyl, TEMPAMINE). Compound 1 is the derivative after reacting TEMPAMINE with an acid chloride.

oxazolidine which has A_N and g-values comparable to nitroxides derived from the Keana synthesis, but gives motion expected of spin labels having enhanced motion about the x-principal axis. These oxazolidines have a hydrogen atom on oxazolidine ring position 5 and as a result have a limited temperature-dependent stability. The half-life for 9,10NS in ethyl oleate at 40 °C is about 2 hr. After loss of signal the decayed compound can be rejuvenated by reoxidizing. At −20 °C 9,10 NS is stable for several weeks or months in the oxidized state.

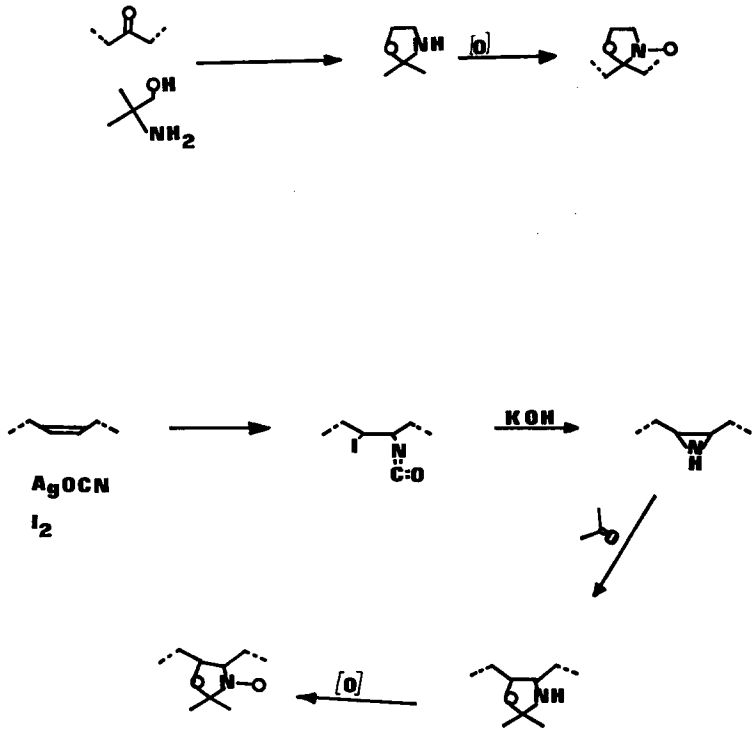

Fig. 2. The top sequence shows the generalized reaction for forming oxazolidines on ketone sites by the Keana synthetic procedure. The second sequence of reactions shows the generalized procedure for putting oxazolidines on double bond sites.

The spin labels presented here represent a variety of molecular geometries which in turn produce a variety of signal types. In treating the signal types these probes generate, we will deal with *molecular motion*, *two component signals*, *matrix-dependent anisotropic motion*, and the *signal differences originating from two structural epimers* of the same compound.

The nomenclature for compounds is listed in the legends for figs. 1 and 3.

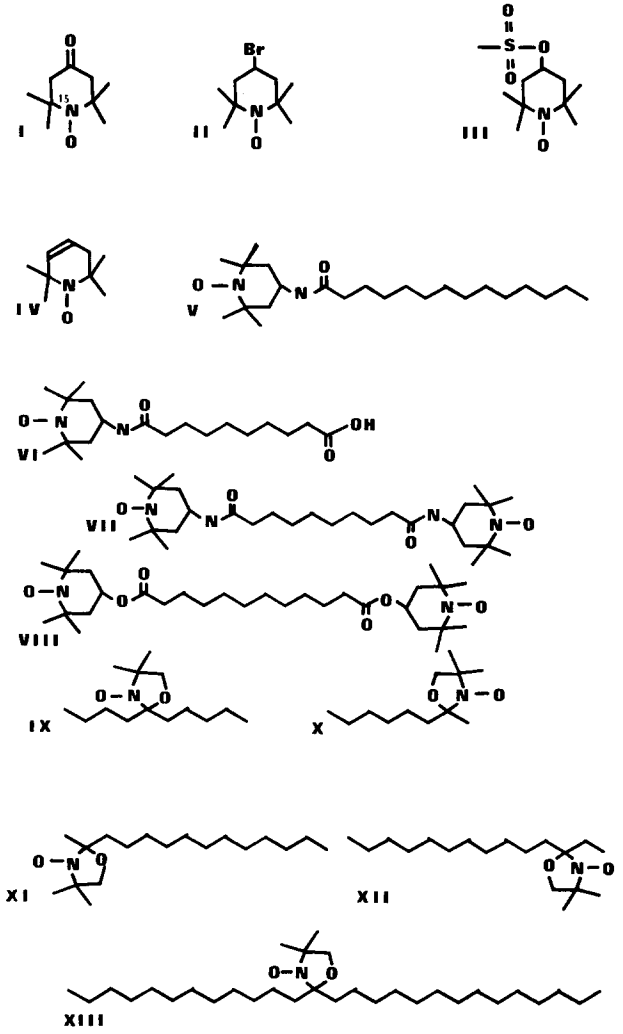

Fig. 3. The structural formulas for spin labels used in the present study are given. – I, 2,2,6,6-tetramethyl piperidone-1-^{15}N oxyl, TEMPONE. – II, 2,2,6,6-tetramethyl piperidine-4Br-1N oxyl, TEMPBr. – III, the methyl sulfonyl derivative of 2,2,6,6-tetramethyl piperidinol-1N oxyl, MST. – IV, 2,2,6,6-tetramethyl piperidine-1N oxyl. – V, the TEMPAMINE derivative of myristic acid, TAM. – VI, the TEMPAMINE half-ester derivative 1,8-dicarboxyl octane, d10:ONT. – VII, the TEMPAMINE biradical of the same fatty acid used in VI, d10:ONT$_2$. – VIII, the di-TEMPOL derivative of 1,10-dicarboxyl decane, d12:OT$_2$. – IX, an oxazolidine is added to carbon 5 of decane, 5 nitroxide decane, 5ND. – X, 2 nitroxide octane, 2NO. – XI, 2 nitroxide tetradecane, 2NT. – XII, 3 nitroxide tetradecane, 3NT, – XIII, 13 nitroxide heptacosane, 13NH. – XIV, 12 nitroxide stearate, 12NS. – XV, 12 nitroxide stearate-9,10-^{3}H, 12NS-9,10-^{3}H. – XVI, the cyclopropane derivative of 12NS, 12NC$_p$S. – XVIII, 4 nitroxide stearate, 4NS. – XVIII, the 9 structural form of 9/10 nitroxide stearate, 9/10NS. – XIX, 5,6-nitroxide stearate and is the same structure as 9, 10NS, except for displacement from the carboxyl group. – XX, 6 nitroxide cholesterol, 6NC. – XXI, the 12 nitroxide stearate ester of cholesterol, 12NS-C. – XXII, 3 nitroxide androstane, α form, 3NA. – XXIII, 13-TEMPOL-heptacosyl ether, 13T27. – XXIV, 9,10-nitroxide stearate, 9,10NS.

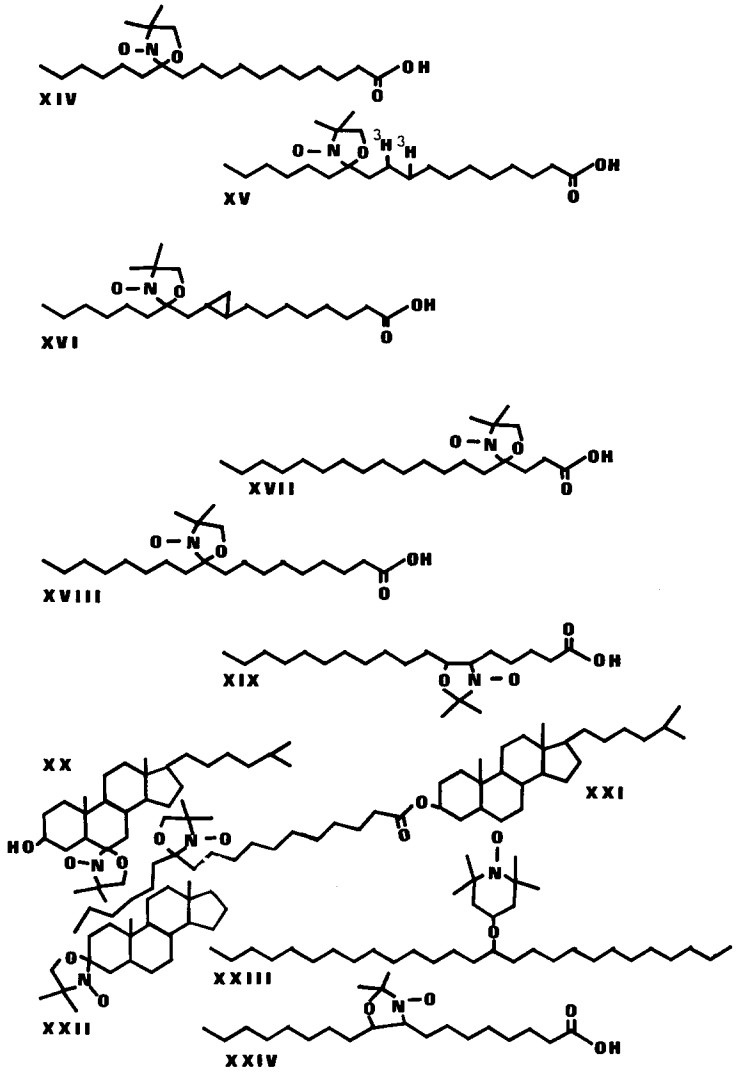

fig. 3(b)

Synthesis of methane sulfonyl TEMPOL (MST) (fig. 3, III):

17.2 g of TEMPOL (0.1 M) was dissolved in 400 ml of dry ether to which was added 20 ml of dry pyridine. 22.4 g of methane sulfonyl chloride (0.2 moles) dissolved in 100 ml of dry ether was dripped into the well-stirred TEMPOL solution over a period of about 1 hr. The solution was allowed to react overnight, filtered over sodium sulfate, and washed with water and bicarbonate solutions. The ether extract was taken to dryness and redissolved

in hexane. Crystallization was carried out at −20 °C; a yield of 22.3 g (91%) was obtained. (Expected, C, 48.0; H, 8.1; N, 5.6; O, 25.6; S, 12.8; observed, C, 47.8; H, 8.1; N, 5.8; O, 25.4; S, 13.0.)

The synthesis of TEMPBr (fig. 3, II):

2.93 g of MST was mixed with 3.0 g of magnesium bromide (anhydrous) in dry ether. The mixture was refluxed overnight, washed with water several times, and crystallized from petroleum ether at −20 °C. This procedure yielded 2.5 g (86% yield) of TEMPBr. Rozantsev et al. have synthesized this compound in lower yield by a different method[17]).

TEMPENE (fig. 3, IV):

1.0 g of TEMPBr was added to 2 ml. of 1,5-diazobicyclo (5.4.0) undec-5-ene (DBU). The mixture was heated in closed glass vial to 80 °C and held at that temperature for 1 hr. The mixture was then extracted with ether and water, the ether washed several times with water, and the ether extract taken to dryness. TLC of the product on silica cel G with chloroform yielded 0.36 g (55% yield). Rozantsev et al. have also synthesized this compound by a different method[17]).

TEMPCl (figs. 1, 7):

3.44 g of TEMPOL was dissolved in 100 ml of anhydrous diethyl ether. To this 7.0 g of PCl_3 in 150 ml of ether was added dropwise. The mixture was allowed to stir for 2 days. The reaction mixture was washed twice with water, taken to dryness, and the precipitate crystallized from petroleum ether. The yield was 1.3 g (34% yield). Alternatively, this compound can be synthesized in the same manner as TEMPBr if $MgCl_2$ is substituted for $MgBr_2$. Rozantsev et al. have synthesized this compound[17]).

Synthesis of 13T27 (fig. 3, XXIII):

The 13-TEMPOL-heptacosyl ether was made by treating 3.92 g of 13-keto heptacosane with 10 equivalents of $LiAlH_4$ overnight in ether while stirring. The ether extracted product was washed twice with sodium bicarbonate and dried under vacuum. 3.2 g of 13-hydroxy heptacosane was dissolved in 500 ml of anhydrous benzene and 12.0 g of powdered KOH were added. This mixture was refluxed using a Dean-Stark water-trap overnight. 1.46 g of MST (0.6 equivalent) was dissolved in 20 ml of benzene and dripped into the refluxing benzene solution over a 2-hr period. The mixture was refluxed for 24 hr and then petroleum ether extracted against bicarbonate aqueous solution. The petroleum ether was washed several times with bicarbonate and

water solutions. The solvent was then evaporated and the sample dissolved in 95% ethanol while gently heating. The ethanol was cooled at 0 °C for 4 days during which the unreacted 13-hydroxy heptacosane crystallized. TLC on silica gel G in chloroform of the final product yielded 0.58 g (approximately 24%).

^{15}N-TEMPONE (fig. 3, I):

Phorone (2.22 g, 0.016 moles) was added to 100 ml of methanol in which 0.4 g sodium (0.9174 moles) had been added. ^{15}N-Hydroxylamine hydrochloride (1 g, 0.0143 moles) was added and the mixture stirred at room temperature for 3 days. The solution was diluted to 1:1 with water, neutralized with HCl and extracted with $CHCl_3$. The extract was dried over Na_2SO_4 and evaporated. KOH (0.84 g, 1.05 eq) in 100 ml of water was added and the solution bubbled with air for 7 days. The resulting pink solution was extracted with $CHCl_3$, dried, and evaporated. Preparative TLC on Silica Gel G in 3:2 ether:petroleum ether gave an ESR positive band of $R_f = 0.30$. Yield 0.08 g (0.3%). This method of synthesis was taken from Lehman[18]).

Biradical synthesis:

Thionyl chloride (24.5 g, 0.22 moles) was added dropwise to a rapidly stirring ether solution of dodecanedicarboxylic acid (5 g, 0.0217 moles) and stirred for 12 hr. The reaction mixture was then refluxed for 2 hr and the solvent removed.

Part of the resulting diacid chloride (1.55 g, 0.0058 moles) was added to two equivalents of pyridine and 2.5 g (0.0145 moles) of TEMPOL in ether and stirred for 6 hr. Washing with $NaHCO_3$ solution, removal of solvent, and preparative TLC in 8:2 $CHCl_3$:acetone resulted in 0.8 g of the half-acid ester and 2.0 g. of the dieester (fig. 3, VIII). Waggoner et al. have synthesized TEMPOL esters[19]).

The remainder of the diacid chloride (4.2 g, 0.0158 M) was added to an ether solution of pyridine (two equivalents) and 7.45 g (0.043 moles) of TEMPAMINE. After stirring for 12 hr, the reaction mixture was oxidized with an ether solution of *p*-chloroperbenzoic acid (3.0 g, 0.0174 moles). After stirring overnight at room temperature, the reaction mixture was washed with $NaHCO_3$ solution and chromatographed on silica gel G plates in 8:2 $CHCl_3$:acetone. The half-acid amide (fig. 3, V) was collected in 0.7 g yield and the diamide yielded 0.3 g. Hsia et al. have made tempamides[6]).

12NO, 12NE$_p$S, 12NA$_c$S:

Ricinoleic acid was used as the starting material for synthesis of substituted 12NS spin labels. An ether solution of methyl ricinoleate (20.0 g, 0.067 moles)

was stirred in an ice bath and bromine (12.8 g, 0.08 moles) added dropwise to achieve bromination of the *cis* double bond. Stirring was continued for 1 hr at room temperature. Solvent and excess bromine were removed on a rotary evaporator to yield 20.0 g of dark red oil (9,10-dibromo-12-hydroxy stearate, A).

The hydroxyl group was oxidized to a ketone by adding CrO_3 (20.0 g, 0.2 moles) in 1 l of glacial acetic acid dropwise to 20.0 g of A in 800 ml of acetic acid stirred in an ice bath. The reaction mixture was allowed to warm to room temperature and stir for a total of 4 hr. An equal volume of water was added, the emulsion extracted with petroleum ether, dried over anhydrous Na_2SO_4, and the solvent removed to yield 15.0 g of oil (9,10-dibromo-12-keto stearate, B).

The ketone B (15.0 g, 0.032 moles) was added to 500 ml of diethyl ether containing 130.0 g (1.46 moles) of 2-methyl 2-amino propanol and 0.2 g of *p*-toluene sulfonic acid. This mixture was refluxed for 5 days with a $CaCl_2$ drying trap, washed with a saturated solution of $NaHCO_3$, dried over anhydrous Na_2SO_4, and the solvent removed to yield 11.5 g. of oil (9,10-dibromo-12-dimethyl oxazolidine stearate, C).

The dibromo-oxazolidine, C, was used as a starting material for the synthesis of the olefin, epoxide, and acetylene analogs, at carbons 9 and 10, of 12NS. In order to obtain the compound containing the double bond, the oxazolidine was oxidized with *p*-chloroperbenzoic acid and then debrominated with acetic acid-zinc. The epoxide was obtained by debrominating first and then performing the oxidation with two equivalents of oxidant. In both cases only a small quantity (<25 mg) was obtained after preparative TLC in 7:3 petroleum ether:ether (12NO, $R_f=0.43$; 12NE_pS $R_f=0.47$) and the material was unstable. Only a trace remained after storage at $-20°C$ for 2–3 weeks.

The acetylene analog of 12NS was prepared by refluxing 0.8 g of C in ethylene glycol containing 0.6 g (0.01 moles) KOH for 12 hr. After cooling, three volumes of water were added, the mixture was neutralized with HCl and extracted with petroleum ether. The dark red-brown oil (0.8 g) obtained was oxidized to yield 0.1 g of ESR positive material after preparative TLC in 1:1 ether: petroleum ether ($R_f=0.30$).

12NC_pS (fig. 3, XVI):

An iodine crystal was added to 7.85 g of zinc-copper couple suspended in absolute ethanol and stirred for 10 min. A mixture of 29.5 g (0.11 moles) of CH_2I_2 and 31.25 g (0.10 moles) of methyl ricinoleate was added dropwise over a period of 1 hr. The reaction mixture was refluxed with a $CaCl_2$ Linde molecular sieve drying trap for 46 hr. After filtration, the solvent was removed

on a rotary evaporator resulting in an oil (29.0 g) (9.10-cyclopropane-12-hydroxy stearate, D).

The cyclopropane fatty acid ester, D (29.0 g) was dissolved in 250 ml of glacial acetic acid and placed in an ice bath. A solution of CrO_3 (0.2 moles) in 500 ml of acetic acid and 50 ml of water was added slowly with vigorous stirring. The reaction mixture was allowed to warm to room temperature and the stirring continued for 24 hr. One liter of water was then added and the solution extracted with petroleum ether. The organic extract was washed with a saturated solution of $NaHCO_3$, dried over anhydrous Na_2SO_4, and evaporated to an oil (27.4 g) (9.10-cyclopropane-12-keto stearate, E).

The cyclopropane, D (5.0 g) was refluxed in toluene with 27.6 g (0.30 moles) of 2-methyl 2-amino propanol and 50 mg *p*-toluene sulfonic acid for 24 hr with a $CaCl_2$ drying trap. The reaction mixture was washed with a saturated solution of $NaHCO_3$ and the solvent removed to give 3.5 g of oil (9.10-cyclopropane-12-oxazolidine stearate, F).

The oxazolidine F (3.5 g) was dissolved in dry ether, placed in an ice bath, and rapidly stirred. To this was added dropwise 20.0 g (0.011 moles) of *p*-chlorobenzoic acid in dry ether. The reaction mixture was allowed to warm to room temperature and stirred for 24 hr. After washing with a saturated aqueous solution of $NaHCO_3$, the solvent was removed. The resulting yellowish oil was chromatographed on silica gel G (according to Stahl) thin-layer plates in 7:3 petroleum ether:diethyl ether. The spin label containing band ($R_f = 0.70$) was collected to yield 1.0 g (25%) of $12NC_pS$.

2-Nitroxide octane (fig. 3, X):

A solution of 2-octanone (5.0 g, 0.04 moles), 26.7 g (0.3 moles) of 2-methyl 2-amino propanol, and 50 mg of *p*-toluene sulfonic acid in toluene was refluxed for 24 hr with a $CaCl_2$ drying trap. The reaction mixture was washed with a saturated $NaHCO_3$ solution, dried, and the solvent removed. The resulting oxazolidine was oxidized with 8.1 g (0.047 moles) of *p*-chloroperbenzoic acid resulting in 5.3 g (50% yield) of yellow oil after preparative TLC on silica gel G in 7:3 petroleum ether:diethyl ether.

9/10 NS (fig. 3, XVIII):

A mixture of 9/100H was obtained from K and K Chemical Co. Synthesis proceeded as for 12NS. Yield was 57%.

12NS-9,10-^3H (fig. 3, XV):

1.0 g of methyl ricinoleate was tritiated with $LiAl^3H_4$ by Nuclear Chicago. Total yield was 6.0 curies. Approximately (8%) of this 0.5 curie was treated by the Keana et al. synthetic procedure[13]). Yield of purified 12NS-9, 10-^3H was 0.04 curies (8%).

TABLE 1

R_f values of nitroxides synthesized*

1. ^{15}N-TEMPONE	0.50	15. 2NO	0.87
2. TEMPBr	0.44	16. 3NA	0.18
3. TEMPCl	0.16	17. 2NA$_d$	0.54
4. MST	0.33	18. 13NH	0.94
5. TEMPENE	0.67	19. 5ND	0.66
6. TAM	0.14	20. 2NT	0.73
7. 10:OT	0.85	21. 12NS-9,10-^{3}H acid	0.17
8. 18:OT	0.91	Me ester	0.85
9. d9:OT$_2$	0.26	22. 12NC$_p$S acid	0.21
10. d12:OT	0.18	Me ester	0.88
11. d12:OT$_2$	0.57	23. 9/10NS acid	0.18
12. d12:ONT	0.17	Me ester	0.89
13. d12:ONT$_2$	0.60	24. 9,10NS (one isomer)	0.18
14. 13T27	0.78	25. 4NS acid	0.05
		Me ester	0.31
		26. 12NS-C	0.20

* On silica gel G in $CHCl_3$

9,10 NS (fig. 3, XXIV):

2.8 g of oleic acid was mixed with 2.5 g of I_2, 3.2 g of AgOCN in 200 ml of anhydrous ether and stirred for 24 hr in the dark at room temperature. The reaction mixture was filtered through anhydrous Na_2SO_4 and taken to dryness in a rotary evaporator. 2.1 g of KOH in 200 ml of anhydrous methanol was added and the mixture was stirred for 24 hr. The mixture was acidified to pH 4.5 with acetic acid, diethyl ether extracted, washed with water, and dried. 200 ml of anhydrous acetone, 10.0 mg of lead acetate, and 10 mg acetic acid were added and the mixture was refluxed for 72 hr using a Dean-Stark trap filled with $CaCl_2$. This mixture was extracted into ether, water washed, dried, resuspended in chloroform, filtered through Na_2SO_4, and purified by thin-layer chromatography on silica gel G. Yield was 0.39 g (9%). This yield percentage represents one of the structural isomers as the aziridine formation results in a mixture of *cis* and *trans*[16]) which undoubtedly carries through to the oxazolidine. (Expected analysis: C, 70.9%; H, 11.6%; N, 3.9%; Observed: C, 70.9%; H, 11.5%; N, 4.0%.)

All experimental spectra were done on a Varian V-4500 X-band spectrometer with a variable temperature attachment.

Isotropic motion:

None of the probes synthesized (fig. 3) are spherical with a totally uniform charge distribution and based on that, none of these would be expected to

give totally isotropic motion. Seelig[20]) has shown that nitroxides which have a polar group anchored in an appropriate matrix such as Asolectin undergo motion which radiates out from the anchoring site. When the anchoring site is close to the N→O group the range of motion is small and increases with distance from the polar site.

Fig. 4A shows a wide range of isotropic motion which resulted from TEMPOL in glycerol at a variety of temperatures from 20 to 100 °C. Fig. 4B shows spectral simulations of isotropic motion over the same approximate range.

Anisotropic motion:

The spin labels 9,10NS and 10:OT (the TEMPOL ester of decanoic acid) have the *x*-principal axis of the N→O group parallel to the long axis of the

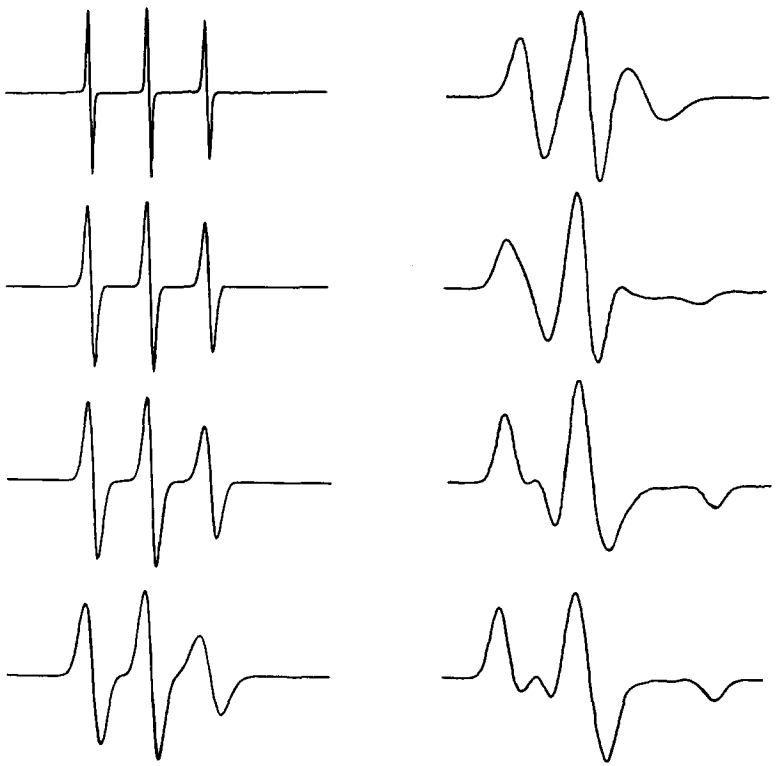

Fig. 4A. Simulated isotropic spectra ranging from the free tumbling state (upper left) to the fully immobilized limit (lower right). The step sizes were chosen as $\Delta\theta_x = \Delta\theta_y = \Delta\theta_z = 0.4$ radian. Beginning with the upper left-hand spectrum, the number of steps and Gaussian lines widths were: 16184, 1G; 4096, 2G; 1924, 3G; 256, 4G; 64, 5G; 16, 5G; 4, 5G; 1, 5G.

parent molecule and would be expected to give enhanced motion about the x-principal axis. Fig. 5 shows spectra in Asolectin (of these two spin labels) at 30 °C and, indeed, the two signals are very similar. 10:OT (fig. 5A) and 9,10NS (fig. 5B) have the same spectral features. On first appearance the

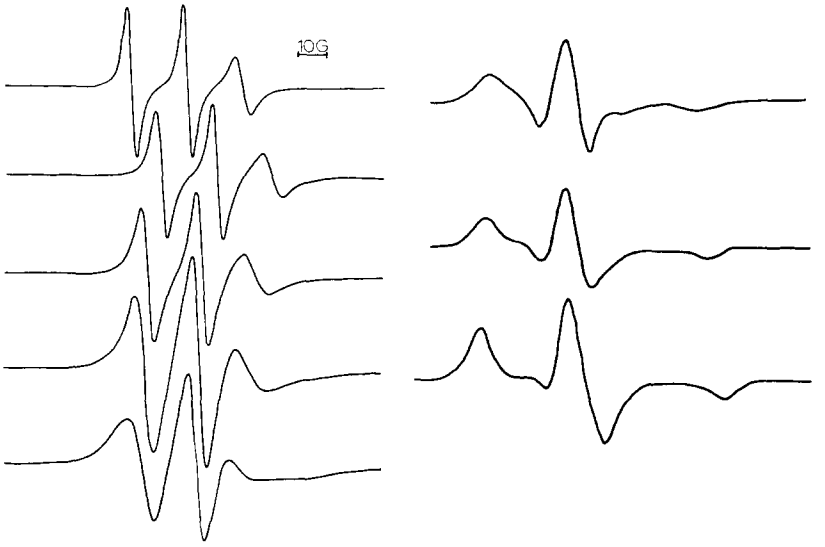

Fig. 4B. Experimental spectra of TEMPOL in glycerol over a temperature range (20–100 °C).

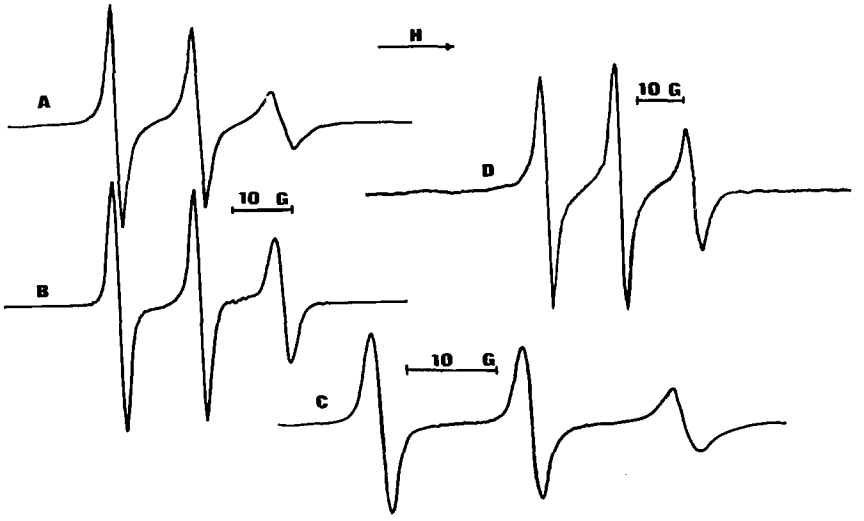

Fig. 5. A, 10:OT in Asolectin at 30 °C. – B, 9.1;NS in Asolectin at 30 °C. – C, TAM in Asolectin at 30°. – D, 12NS in Asolectin at 50 °C.

structure of 9,10NS looks much like that of 9/10NS, at least when viewed on a planar diagram such as that shown in fig. 3; however, the oxazolidine rings are turned 90° to each other with respect to the fatty acid chain. This causes the $(y+z)$ anisotropic contributions to tumble with enhanced velocity in 9,10NS and the $(y+x)$ anisotropic contributions to tumble with enhanced velocity in 9/10NS. Fig. 5C shows 10:OT in dimethyl-sulfoxide which is a relatively isotropic matrix: therefore, the anisotropic motion emanating from this spin label is not matrix dependent. A representative isotropic signal is given by 12NS in Asolectin at 60° (fig. 5D). The general character of x-axis anisotropic motion can be defined as ω_x, where h_1 and h_0 are the high and mid field line heights

$$\omega_x = \frac{h_1}{h_0}$$

and is unambiguous when $\omega_x > 1$. Simulations of spin label motion are consistent with this frame of reference. All the spin labels having the x-principal axis parallel to the long axis of the parent molecule are expected to yield this type of anisotropic motion (x-axis anisotropy).

The spin label 3NA (fig. 3, XXII) shows a different type of symmetry such that the y-principal axis is parallel to the fast tumbling axis of motion of the 3NA molecule. Here, the $(x+z)$ principal axis contributions have enhanced time-dependent averaging and result in a ω_y closer to one than would result from isotropic motion, where $\omega_y = h_1/h_{-1}$. The structure of this spin label complicates the expected motion since two epimers exist (figs. 7, 8).

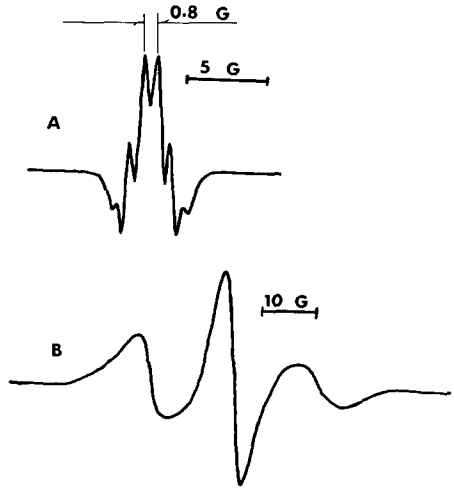

Fig. 6. A, mid-line fine structure for the (A) epimer of 3NA taken in degassed n-butane at 40°C. – B. the ESR signal originating from either epimer (A) or (B) in Asolectin at 30°C.

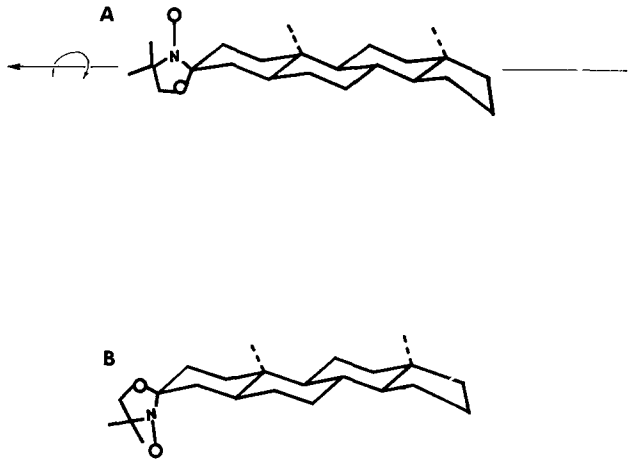

Fig. 7. (A) and (B) are the two expected geometric isomers originating from the synthesis of 3NA Either epimer is expected to rotate on the *y*-principal axis of the nitroxide.

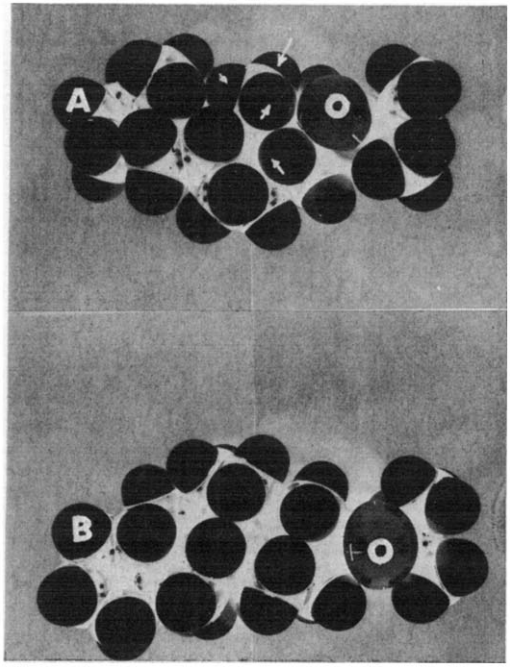

Fig. 8. The arrows on epimer (A) show the proximity of three hydrogens attached to a methyl group and another single hydrogen which are apparently close enough to split the ^{14}N hyperfine line into fine structure shown in fig. 6. The (O) in both (A) and (B) refers to the oxygen molecule of the N-oxyl group. The nitrogen atom is buried behind the oxygen atom. Epimer B shows that the N→O group is equally spaced from all hydrogens and is not in as close a proximity to any hydrogen as epimer (A).

These two epimers are both expected to yield approximately y-axis anisotropy even though the N→O group is localized in different environments. (A) epimer has a more hydrogen-rich domain and, as expected, results in more complex hyperfine splittings. The signal shown in fig. 6A resulted from 3NA in degassed n-butane and shows only the mid-line. All three lines show the same fine structure; however, they are better resolved in the mid-line. Epimer A shows this fine structure while epimer B has no fine structure. Both give a signal in Asolectin which results in y-axis anisotropy (fig. 6B).

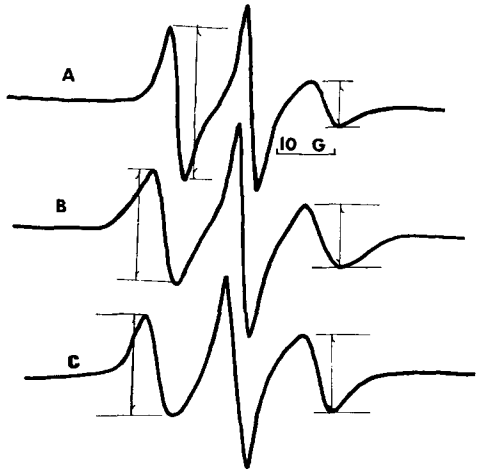

Fig. 9. A, the isotropic spectrum derived from 13NH in dimethylsulfoxide. – B, the y-axis anisotropic motion spectrum derived from 13NH in Asolectin. – C, the y-axis anisotropic spectrum derived from 3NA in dipalmitoyl phosphatidyl choline.

Fig. 9A shows 13NH (fig. 3, XIII) in dimethylsulfoxide and reflects an isotropic signal. Fig. 9B shows 13NH in Asolectin where it now has some character of y-axis anisotropy. Contrary to that stated for 10:OT earlier, this spin label demonstrates some matrix-dependency and has an ω_y of about a factor of two, different from what would be expected of isotropic motion.

Fig. 10 shows 9,10NS under different matrix conditions. Fig. 10A shows 9,10NS in dimethylsulfoxide and here reflects an isotropic signal. Fig. 10B shows 9,10NS in Asolectin and under these conditions x-axis anisotropy results. Fig. 10C shows 9,10NS in ethyl oleate and, again, demonstrates x-axis anisotropy. Therefore, 9,10NS shows anisotropy dependent upon matrix molecular geometry, 13NH shows anisotropy dependent upon polar zones, and 10:OT shows matrix independent anisotropic motion.

Fig. 11A shows spectral simulations about the x-principal axis and in fig.

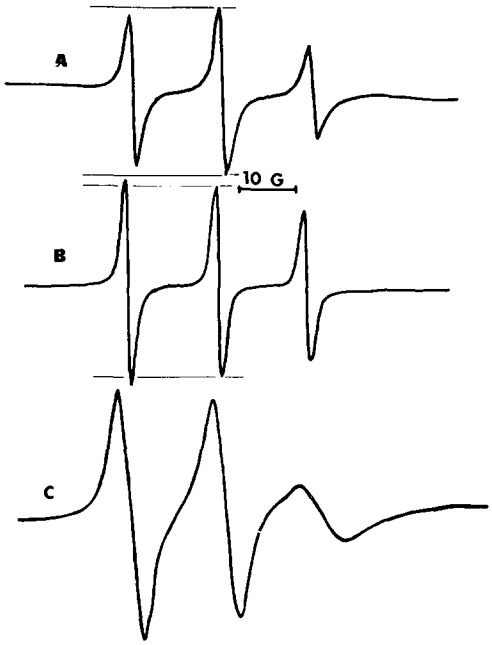

Fig. 10. A, the isotropic signal derived from 9.10NS in dimethylsulfoxide at 0°C. – B, the x-axis anisotropic signal derived from 9,10NS in Asolectin at 45°C. – C, the x-axis anisotropic signal derived from 9,10NS in ethyl oleate at 10°C.

11B about the y-principal axis. The rationale for these simulations will be explained under *spectral simulations.*

Heterogeneous environments and mixed signals:

In biological systems these would originate from polarity, viscosity, and effective radius effects. If a spin label is partitioned between two different viscosities, three narrow lines will be seen superimposed on three broad lines. Of course, the partitioning of signals must be in a range where both have the same order of amplitude intensity (height, h). The integrated intensity (I_i) is expressed as $I_i = kW^2h$ for Lorentzian line shapes, where k is a constant. Consequently, when both have equal height, the broader line has considerably greater I_i and care must be taken in making quantitative statements about multicomponent signals.

Signals originating from two zones of different polarities but viscosities which are not grossly unequal usually have two high-field lines and the relative heights may be concentration-dependent (fig. 12). This originates due to alterations in the g-scalar and hyperfine coupling terms.

A simulation of this spectral type is shown in fig. 13. One signal may be

considerably more immobilized than the other signal, where the two originate from two binding sites with one relatively tight and the other relatively loose.

More subtle heterogeneous effects may occur which do not result in two discrete signals superimposed on each other. For example, when the spin label is distributed along a polarity or viscosity gradient the signal will not be representative of any discrete state of motion. Particularly with polarity

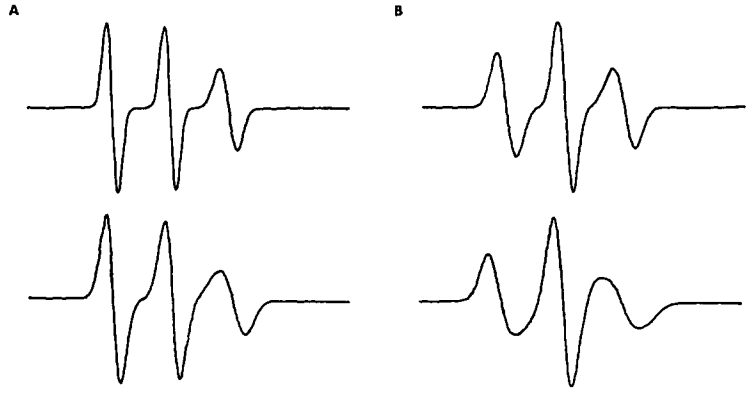

Fig. 11. A, shows simulated spectra for enhanced tumbling about the x-axis. For the upper spectrum the step sizes were $\Delta\theta_z = \Delta\theta_y = 0.8$ radian and $\Delta\theta_x = 3.2$ radians, while the line width was 3G. The lower spectrum was gnerated with $\Delta\theta_z = \Delta\theta_y = 0.4$ radian, $\Delta\theta_x = 1.6$ radians and a line width of 4G. – B, represents y-axis anisotropy with the upper spectrum given by $\Delta\theta_z = \Delta\theta_x = 0.4$ radian, $\Delta\theta_y = 1.6$ radians, and a line width of 4G and the lower spectrum having $\Delta\theta_z = \Delta\theta_x = 0.2$ radian, $\Delta\theta_y = 0.8$ radian, and a line width of 5G. For all these simulations 64 steps were used.

averaging, considerable line broadening may occur which broadens the three lines unequally and will cause distortions in the measurable τ_c by the Kivelson method. It is not possible at this time to state the precise natural line width contribution associated with a given degree of immobilization for the spin label 12NS or any of the oxazolidine nitroxides. Fig. 14 shows an example of two spectra, (A) was the result of the acid of 12NS being dispersed in a 0.3% solution of potassium oleate. This spectrum shows very narrow lines and has an almost identical h_0/h_{-1} ratio to that of the spectrum (B) shown below it which was taken in Asolectin employing the same spin label. However, the line widths are very different. We imagine that a dispersion of Asolectin would present heterogeneity effects due to a variety of causes. First of all, the vesicle size represents a range of sizes from perhaps 200 Å in diameter to several thousand angström in diameter. Bilayers trapped in the very large vesicles may allow different states of motion of the individual phospholipid molecules than are allowed by the very small vesicles. There are probably

several other complexities that would result in heterogeneity effects in this type of system. We believe that the problem of spin labeling biological membranes also results in heterogeneity since the lines are always broadened to some extent even when the h_0/h_{-1} is less than two or three. From the work which our laboratory has carried out on the spin labeling of biological membranes using the spin label 12 NS, it appears that there is still considerable information and that these line measurements may be, in fact, plotted on Arrhenius plots using either τ_c or τ_0.

$$\tau_c = K(W_{-1} - W_0) = KW_0\left[\left(\frac{h_0}{h_{-1}}\right)^{\frac{1}{2}} - 1\right].$$

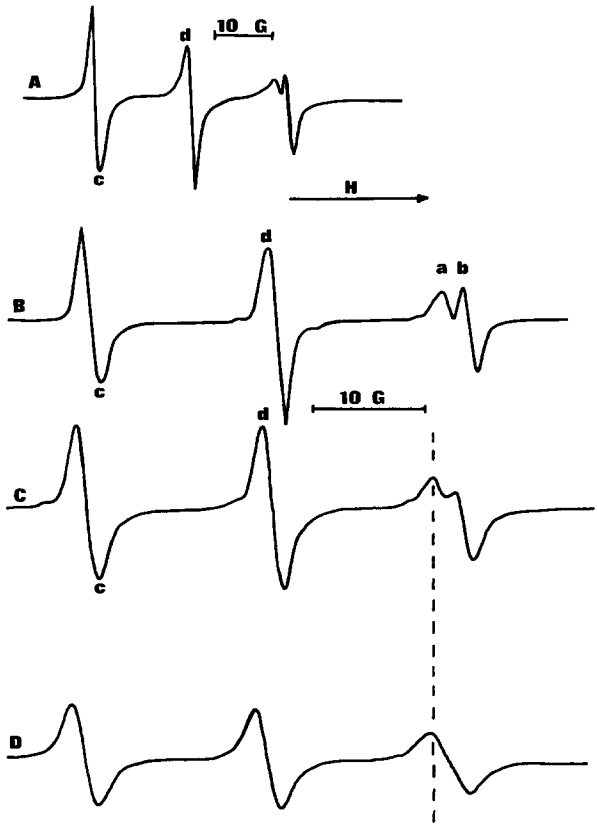

Fig. 12. A, the spectra resulting from 13T27 dissolved in Asolectin at 8×10^{-4}M. – B, 13T27 in Asolectin at 4×10^{-4}M. – C, 13T27 in Asolectin at 2×10^{-4}M. – D, 13T27 in Asolectin at 10^{-4}M. The small *a* and *b* shows the characteristic two 3rd-line character, which results from arithmetic addition of two different sets of *g*-values and A_N values. The small *c* and *d* shows the distorted line shapes which typically results from addition of two sets of *g*-values and A_N values.

When τ_c is $>10^{-9}$ sec, then the notation τ_0 is used as an empirical approximation for purposes of Arrhenius graphs. τ_c is the rotational correlation time, W_0 is the mid-line width, W_{-1} is the high-field line width, h_0 is the mid-line height, h_{-1} is the high-field line height and K is a constant which depends on the anisotropic hyperfine couplings (A_x, A_y, A_z) and g-tensor terms

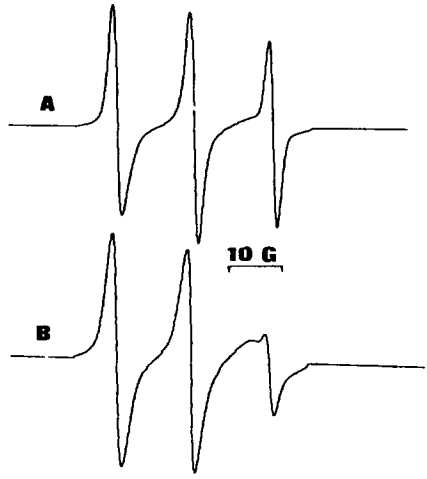

Fig. 13. Simulated composite spectra. Lorentzian line widths were computed with the Kivelson formula for isotropic motion. One spectrum of the sum was generated with an isotropic g-value of 2.0059, an isotropic hyperfine coupling of 16.6G, and a correlation time of 10^{-11} sec. For the other $\bar{g} = 2.0054$, $\bar{T} = 14.9$G and $\tau_c = 4 \times 10^{-10}$ sec. For A the intensities are 1:2 and for B 1:12, respectively. Line asymmetry is the most striking feature of non-homogeneity in A.

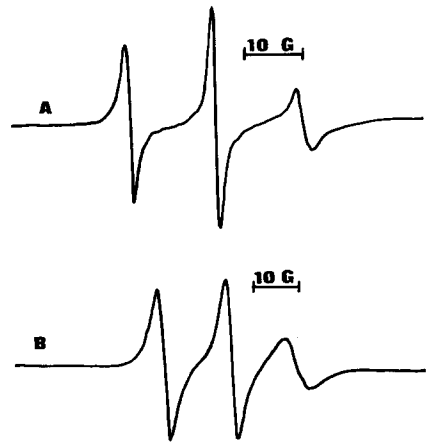

Fig. 14. A, the spectrum which results from the acid of 12NS solubilized by 0.2% potassium oleate at 14°C. – B, the spectrum which results from the acid of 12NS dissolved in Asolectin at 25°C. Both are at 2×10^{-4}M of 12NS bulk concentration.

(g_x, g_y, g_z). The spectral parameters of Griffith et al.[21]) are used and the equation for τ_c can be derived from Kivelson[22]).

Spectral simulations:

Simulations were performed by an elaboration of the Monte Carlo method first employed by Itzkowitz[23]). This procedure can be regarded for present purposes as a mathematically convenient model for dscribing the observed time averaging of the anisotropic Hamiltonian of the tumbling nitroxide molecule. The usefulness of the method will be demonstrated with reference to spectra of well-characterized model systems.

To simplify the treatment of anisotropic motion, the tumbling motion of the nitroxide was generated by means of Eulerian rotations about the principal axes of the molecule. The step size about the ith axis was chosen from a set of random numbers uniformly distributed between $\pm \Delta\theta_i$. A single jump of the molecular motion was produced by the matrix operation

$$\begin{pmatrix} x^1 \\ y^1 \\ z^1 \end{pmatrix} = \begin{pmatrix} \cos \Delta_z & \sin \Delta_z & 0 \\ -\sin \Delta_z & \cos \Delta_z & 0 \\ 0 & 0 & 1 \end{pmatrix} \begin{pmatrix} \cos \Delta_y & 0 & \sin \Delta_y \\ 0 & 1 & 0 \\ -\sin \Delta_y & 0 & \cos \Delta_y \end{pmatrix} \times \begin{pmatrix} 1 & 0 & 0 \\ 0 & \cos \Delta_x & \sin \Delta_x \\ 0 & -\sin \Delta_x & \cos \Delta_x \end{pmatrix} \begin{pmatrix} x \\ y \\ z \end{pmatrix}, \quad \text{where} \quad \begin{pmatrix} x \\ y \\ z \end{pmatrix}$$

represents the orientation vector of the nitroxide molecule relative to the laboratory magnetic field. The line positions relative to the isotropic g-value were computed with the formula[24])

$$E(M) = g_x \sin^2\theta \cos^2\theta + g_y \overset{S}{\sin}{}^2\theta \sin^2\theta + g_z \cos^2\theta + M\,(T_x^2 \sin^2\theta \cos^2\theta + T_y^2 \sin^2\theta \sin^2\theta + T_z^2 \cos^2\theta)^{\frac{1}{2}},$$

where $M = -1, 0, +1$ for ^{14}N and $M = -\frac{1}{2}, +\frac{1}{2}$ for ^{15}N. While these energies differ slightly from those expected for the fast tumbling region, they are adequate for the qualitative purposes of this paper. The tensors were those found by Hubbell[17]) for the N-oxyl-4′, 4′-dimethyl-oxazolidine derivative of 5α-cholestan-3-one. These are

$$g_x = 0.0033,\ g_y = 0.0002,\ g_z = -0.0035$$
$$T_x = 30.8\,G,\ T_y = 5.8\,G,\ T_z = 5.8\,G\,(X\text{-}band).$$

Using the nuclear moment ratios the hyperfine parameters for ^{15}N are computed to be

$$T_x = 43.3\,G,\ T_y = 8.2\,G,\ T_z = 8.2\,G\,(\text{X-band}).$$

Isotropic tumbling modes were simulated by setting $\Delta\theta_x = \Delta\theta_y = \Delta\theta_z = 0.4$ radians and varying the number of steps as indicated in fig. 1. Both ^{14}N and ^{15}N spectra were calculated in this manner and displayed by means of the CAL-COMP plotter. All spectra were modulated using the gaussian function $1/r_0\, e^{-2\times 2/r_0^2}$, where r_0 corresponds to the effective line width of an ensemble of molecules having a given line position.

Spectra showing a wide range of experimental and simulated isotropic motion are shown in fig. 4A for an ^{14}N-nitroxide and in fig. 15B for an ^{15}N-nitroxide. Fig. 15A illustrates the natural abundance contributions from ^{13}C and ^{15}N in ^{14}N-TEMPONE. The natural line width of TEMPONE in water is about 0.4 gauss and the ^{13}C induced contributions are split by about 5 g. In fig. 15A spectra B-F illustrate the spectral changes which result from ^{15}N-

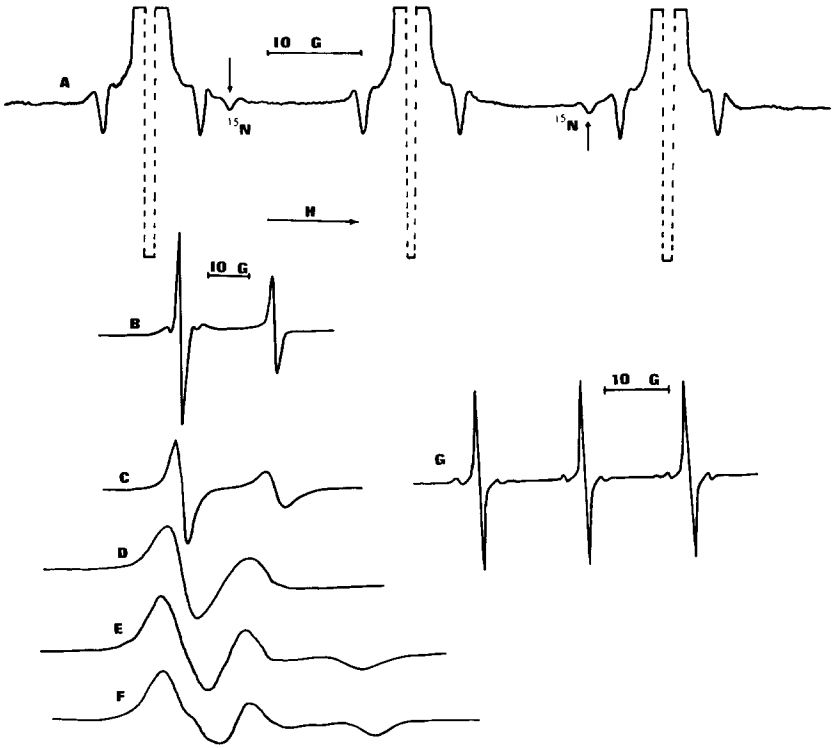

Fig. 15A. A, the second derivative spectrum which results from TEMPONE dissolved in water at room temperature. The arrows point to the natural abundance contribution from ^{15}N. The two lines on either side of the major three hyperfine lines represent the contributions made by the natural abundance of carbon 13. – B–F, show the spectral changes which results in ^{15}N-TEMPONE dissolved in glycerol at temperaturs ranging from 20 to 100°C. – G, a first derivative spectrum of ^{14}N-TEMPONE taken on the same spectral scale as B to illustrate the coupling differences.

TEMPONE in glycerol over the temperature range 20–100 °C. The qualitative agreement with the simulations is good, indicating that the time averaging method is a good first order representation of observed isotropic spectra essentially in terms of a single parameter: N, the number of steps of the tumbling motion.

Two types of anisotropic motion were treated by fixing the number of steps and varying the step size as shown in fig. 11. The differences between these simulations and those of isotropic motion are striking enough to be recognizable experimentally. This can be seen in fig. 11, where spectra of x- and y-axis anisotropy are shown. The geometry of the nitroxides indicates that enhanced averaging about the given nitroxide principal axis can be expected to occur (refer to fig. 3 for structures). Simulations of enhanced averaging about the z-axis are essentially identical to those of isotropic tumbling and details of that spectral type will not be dealt with here.

Composite spectra arising from environments of different polarity or viscosity are often observed in biological preparations. One approach to

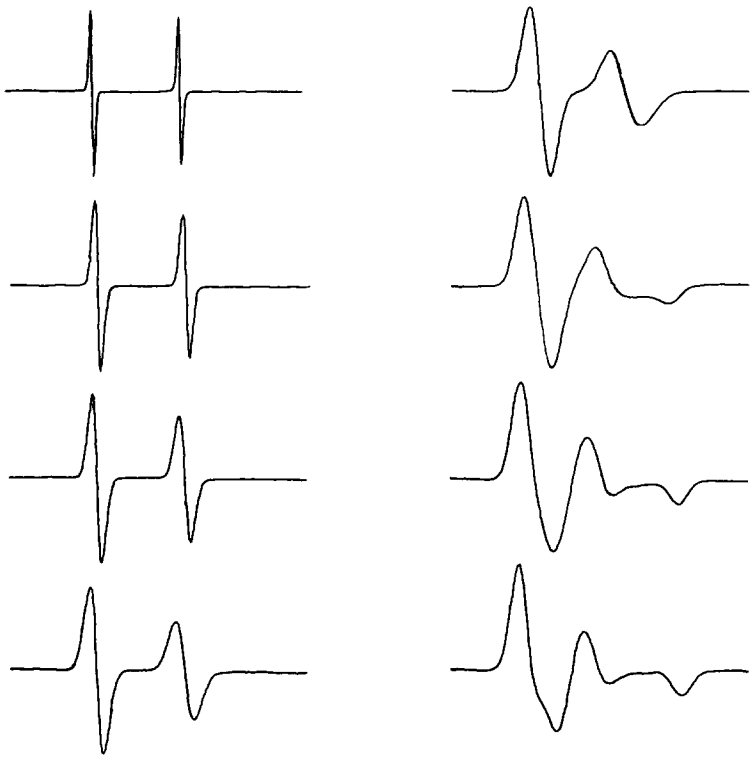

Fig. 15B. Simulated isotropic spectra for an ^{15}N nitroxide. Step parameters are identical to those of fig. 4A.

analyzing these spectra is to add simulated spectra and thus infer quantitatively the partitioning between different environments. An example of this approach is given in fig. 13, showing a composite of polar and non-polar environments. Lorentzian line widths were determined by the Kivelson equation[22]) and were used for these simulations since the Monte Carlo method becomes very demanding of computer time near the fast tumbling limit. One important application of such simulations will be to study temperature dependent partitioning of nitroxides between interior and exterior regions of biological membranes. Compartmentalization of ^{14}N and ^{15}N probes exploiting concentration broadening represents another important potential application of two component computer simulations.

III. Discussion

Previously, factors such as A_N, g, τ_c and heterogeneity have been used to derive information as to the polarity and viscosity of biological matrices. Seelig qualitatively described the spectral changes resulting from the variation in the distance between the spin moiety and the polar anchoring site in alkyl chains[20]). Although we presented examples of resolving structural isomers, as in 3NA, by ESR hyperfine structure and the use of ^{14}N and ^{15}N for simultaneous probing of different environments in a matrix, our primary purpose is to propose a new ESR parameter. There is great potential of deriving useful information from some anisotropic index. The demonstration of matrix dependency illustrates the value of this index in studying order in biological matrices as can be readily seen in the case of 9,10NS, this parameter also serves as a structure proof and establishes that a given type of motion is dependent on spin label geometry.

Thus, consideration of molecular geometry and electron orbital orientation in the design of spin label probes and an understanding of the resulting spectra in terms of an anisotropic index greatly expands the knowledge obtainable from ESR studies of biological matrices.

Acknowledgements

This work was supported by grants from the U.S. Atomic Energy Commission and the U.S. Public Health Service (AM-12939).

References

1) P. Jost, L.J. Libertini, V.C. Hebert and O.H. Griffith, in manuscript.
2) L.J. Libertini, A.S. Waggoner, P.C. Jost and O.H. Griffith, Proc. Natl. Acad. Sci./U.S. **64** (1969) 13

3) J.C. Hsia, H. Schneider and I.C.P. Smith, Biochim. Biophys. Acta **202** (1970) 399
4) W.L. Hubbell and H.M. McConnell, Proc. Natl. Acad. Sci. U.S. **64** (1969) 20
5) W.L. Hubbell and H.M. McConnell, Proc. Natl. Acad. Sci. U.S. **63** (1969) 16
6) J.C. Hsia, H. Schneider and I.C.P. Smith, Chem. Phys. Lipids **4** (1970) 238
7) K.W. Butler, I.C.P. Smith and H. Schneider, Biochim. Biophys. Acta **219** (1970) 514
8) P. Jost and O.H. Griffith, in: Methods in pharmacology, Vol. 2: Physical methods in pharmacology, ed. by C. Chignell. Appleton-Century-Crofts, New York (1971)
9) I.C.P. Smith, in Biological applications of electron spin resonance spectroscopy, ed. by J.R. Bolton, D. Borg and H. Schwartz. Interscience, JohnWiley and Sons, New York (1970)
10) H.M. McConnell and B.G. McFarland, Quart. Rev. Biophys. **3** (1970) 91
11) W.J. Baumann and H.K. Mangold, J. Org. Chem. **29** (1964) 3055
12) W.J. Baumann and H.K. Mangold, J. Lipid Res. **1** (1966) 568
13) J.F.W. Keana, J.B. Keana and D. Beetham, J. Am. Chem. Soc. **49** (1967) 3055
14) L. Birkenbach and M. Linhard, Ber. **63** (1930) 2544
15) A. Hassner, M.E. Lorber and C. Heathcock, J. Org. Chem. **32** (1967) 540
16) N.J. Leonard, J.V. Paukstelis and L.E. Brady, J. Org. Chem. **29** (1964) 3383
17) E.G. Rozantsev, V.A. Golubev and M.B. Nieman, Izv. Akad. Nauk SSSR, Ser. Khim. (1965) 391
18) F. Lehmann, Ber. **30** (1897) 2736
19) A.S. Waggoner, A.D. Keith and O.H. Griffith, J. Phys. Chem. **72** (1968) 4219
20) J. Seelig, J. Am. Chem. Soc. **72** (1970) 3881
21) O.H. Griffith, D.W. Cornell and H.M. McConnell, J. Chem. Phys. **43** (1965) 2909
22) D. Kivelson, J. Chem. Phys. **33** (1960) 1094
23) M.S. Itzkowitz, J. Chem. Phys. **46** (1967) 3048
24) L.J. Libertini and O.H. Griffith, J. Chem. Phys. **53** (1970) 1359